IEEE Robotics and Automation Letters (RAL) paper presented at the
2020 IEEE International Conference on Robotics and Automation (ICRA)
31 May - 31 August, 2020. Paris, France

Gyroscopic Tensegrity Robots

Raman Goyal[1], Muhao Chen[1], Manoranjan Majji[2], and Robert E. Skelton[2]

Abstract— Mechanics and control of innovative gyroscopic structural systems are detailed in the paper. By adding controllable spinning wheels to a network of controllable, axially loaded strings and bars, it is shown that the mobility and manipulation of the structural system are enhanced. Using principles of mechanics, a nonlinear dynamic model is presented to modulate the torque produced by the network of spatially distributed gyroscopes. Equations of motion, formulated as a second-order matrix differential equation, provide a trajectory for the nodal displacement of the bars, along with the wheel's spin degree of freedom. While the gyroscopic robotics concept is scalable to an arbitrarily large network, this research aims to identify elemental modules to override fundamental design principles of the innovative structural systems. Dynamic simulation and experimental verification on a planar D-bar tensegrity structure are used to demonstrate the utility of one such fundamental building block of the gyroscopic robotic system.

Index Terms— Soft Robot Applications, Dynamics, Space Robotics and Automation

I. Introduction

Tensegrity structures are defined as a stable configuration of pre-stressable structures composed of compressive (bars/struts) and tensile members (strings/cables). The word is conjugated from "tension" and "integrity", and was originally used for art and architectural applications by Kenneth Snelson [1]. Recent research found remarkable engineering applications of tensegrity structures [2]. These applications can be attributed to the fact that several fundamental problems in engineering mechanics are solved by various structural topologies of tensegrity structures. Light-weight and deployable space structures [3], [4], tunable meta-materials [5], and compliant soft robots [6], [7], [8] are some applications of interest [9]. Researchers also show that tensegrity structures provide a minimal mass solution to structures designed for compressive loading [2] and tensile loading under stiffness constraints [10]. These structures also provide the capability to change the stiffness without changing the shape of the structure. This can help in achieving a high range of compliance in soft robotics applications [8]. A large number of redundant control inputs (tension in the strings) makes the system robust, which is crucial for next-generation robots. Harvard biologist Don Ingber called tensegrity architecture as 'architecture of life' [11], which is evident by examining the human body where the tensions in the tendons actuate bones of the skeleton. All the above-mentioned properties make tensegrity suitable for optimal, robust, and precise control of soft robots.

An extra degree of control can be added to these systems by attaching gyroscopic wheels to some of the bar members. This paper discusses this new class of mechanical systems formed by adding gyroscopes to tensegrity structures. This has been mentioned in the past but has not been described in detail [12]. Spacecraft attitude and orientation control are typically accomplished using momentum wheels or control moment gyroscopes [13], [14]. Gyroscopes have been used to minimize the sensitivity of the end-effector location in the presence of disturbance forces [15]. In large space structures such as the international space station, massive monolithic wheels are arranged on steerable gimbals, to generate gyroscopic torques in order to accomplish attitude control [16], [17]. Motivated by the expense of large masses in space, we ask the fundamental question as to what would be an optimal arrangement of mass distribution of the rotational kinetic energy, so as to maximize the efficacy of the gyroscopic torques generated by the system. While this is an open question, the tensegrity paradigm provides a framework to provide a systematic answer to this question. The ability to harness a gyroscopic torque by executing translational pivoting motion of the bars, equipped with rotating wheels, provides a new modality of structural system mobility and manipulation. While space structures such as the habitats are positively impacted, a variety of terrestrial applications are also affected by a systematic development of tools for mechanics and control of gyroscopic systems [18]. Building on these foundations, the optimal utilization of the control redundancy introduced by the spatial distribution of the gyroscopes will be possible. A typical actuator redundancy present in traditional tensegrity systems along with the added control of gyroscopic forces will allow for the accommodation of a wide variety of disturbance forces encountered in practical robotic applications making the system more robust. In order to affect moment transfer, it is necessary that the tensegrity structures be of class 2 or greater, so as to efficiently transfer the reaction moments to the subsystem of interest. This paper formulates a matrix-second-order nonlinear differential equation without any transcendental functions to simulate the dynamics of a general tensegrity system with or without gyroscopes.

[1]Raman Goyal and Muhao Chen are graduate students with the Department of Aerospace Engineering, Texas A&M University, College Station, USA. ramaniitrgoyal92@tamu.edu, chenmuhao0911@tamu.edu

[2]Manoranjan Majji and Robert E. Skelton are faculties with the Department of Aerospace Engineering, Texas A&M University, College Station, USA. mmajji@tamu.edu, bobskelton@tamu.edu

The advantages of the formulation and the contributions of this work are summarized as follows:

- There are no topological constraints (rigid body connections to form a topological tree) as non-minimal representation is used in the formulation.
- The absence of transcendental functions results in improved efficiency and accuracy of the dynamics simulation and control design.
- This work systematically derived the dynamics of a general gyroscopic tensegrity system, which provides an extra degree of freedom to control the shape and attitude of the structure.
- These equations are suitable for the design of control law to control the shape and attitude of the structure as the control variables (force density in each string) are linear in the dynamics formulation.

The paper is structured as follows: Section 2 introduces the notation and provides the kinematic rules used throughout the paper. Section 3 develops the equations for rotational and translational motion of a rigid bar with an attached wheel. Section 4 provides the complete dynamics formulation for any gyroscopic tensegrity structure in a compact second-order matrix differential equation along with a vector differential equation to capture the angular position of the wheel. In section 5, the reduced-order dynamic model for class-k tensegrity system is developed by projecting the constrained space to a smaller subspace. A physical model of planar D-bar structure [2] with gyros attached to each member is first described, and then an experiment is run to show the application of the proposed work in controlling the attitude of the structure by changing the shape (by controlling the length of the strings). Section 6 also provides the results developed from the dynamic simulation validating the experiment. Finally, the conclusions and brief discussion about the paper are given in section 7.

II. Notation and Kinematics

Let us define a Vectrix $\boldsymbol{\mathcal{E}} = \begin{bmatrix}\boldsymbol{e}_1 & \boldsymbol{e}_2 & \boldsymbol{e}_3\end{bmatrix}$ [14] as a matrix containing a dextral set ($\boldsymbol{e}_1 \times \boldsymbol{e}_2 = \boldsymbol{e}_3, \boldsymbol{e}_2 \times \boldsymbol{e}_3 = \boldsymbol{e}_1$) of unit vectors $\boldsymbol{e}_i$ that are inertially fixed and a Vectrix $\boldsymbol{\mathcal{B}} = \begin{bmatrix}\boldsymbol{b}_1 & \boldsymbol{b}_2 & \boldsymbol{b}_3\end{bmatrix}$ as a matrix containing a body-fixed dextral set of $\boldsymbol{b}_i$ fixed in the principal coordinates of the rigid body defined as:

$$\boldsymbol{\mathcal{B}} = \boldsymbol{\mathcal{E}}\Theta, \quad \Theta \rightarrow \text{Direction Cosine Matrix (DCM)}.$$

The components of the vector $\boldsymbol{v}$ are represented in frame $\boldsymbol{\mathcal{E}}$ and $\boldsymbol{\mathcal{B}}$ as $v^{\mathcal{E}}$, $v^{\mathcal{B}}$, such that:

$$\boldsymbol{v} = \boldsymbol{\mathcal{E}} v^{\mathcal{E}} = \boldsymbol{\mathcal{B}} v^{\mathcal{B}}, \quad v^{\mathcal{E}} = \Theta v^{\mathcal{B}}, \tag{1}$$

and the angular velocity of the frame $\boldsymbol{\mathcal{B}}$ w.r.t. frame $\boldsymbol{\mathcal{E}}$ is defined as:

$$\boldsymbol{\omega} = \boldsymbol{\mathcal{E}}\omega^{\mathcal{E}} = \boldsymbol{\mathcal{B}}\omega^{\mathcal{B}}. \tag{2}$$

Then vector $\boldsymbol{v}$ and its inertial derivative $\dot{\boldsymbol{v}}$ are written as:

$$\boldsymbol{v} = \boldsymbol{\mathcal{B}} v^{\mathcal{B}}, \tag{3}$$

$$\dot{\boldsymbol{v}} = \dot{\boldsymbol{\mathcal{B}}} v^{\mathcal{B}} + \boldsymbol{\mathcal{B}}\dot{v}^{\mathcal{B}} = \boldsymbol{\mathcal{B}}[\tilde{\omega}^{\mathcal{B}} v^{\mathcal{B}} + \dot{v}^{\mathcal{B}}], \tag{4}$$

where $\Theta^{\mathsf{T}}\dot{\Theta} = \tilde{\omega}^{\mathcal{B}}$ was used as the property of DCM and $\tilde{\omega}^{\mathcal{B}}$ is a skew-symmetric matrix generated using the elements of the vector $\omega^{\mathcal{B}}$.

III. Dynamics of a Bar with Wheel

In this section, we develop the dynamics of a rigid bar with an attached wheel. The rigid bar is defined as an axisymmetric body with no inertia about the longitudinal axis. It is also assumed that the bar is subjected to external forces only at its two ends. We use the notations and kinematics developed in our recent paper [19] to formulate the dynamics. Let us define $\boldsymbol{b}$ as a vector along the bar and vector $\boldsymbol{r}$ representing the position vector of the center of mass of the bar, as shown in Fig. 1.

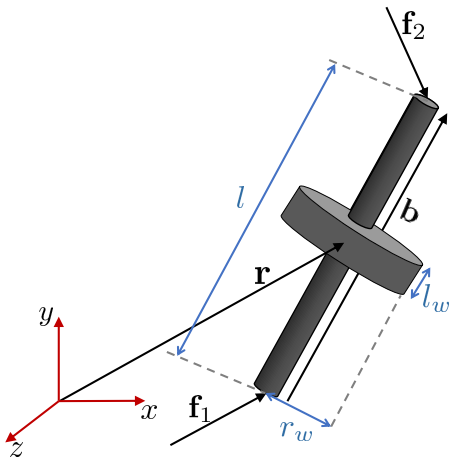

Fig. 1. Tensegrity bar member vector nomenclature.

The bar vector $\boldsymbol{b}$ is described in body coordinates $\boldsymbol{\mathcal{B}}$ as:

$$\boldsymbol{b} = \boldsymbol{\mathcal{B}} b^{\mathcal{B}}, \quad b^{\mathcal{B}} = \begin{bmatrix}0 & 0 & l\end{bmatrix}^{\mathsf{T}}, \tag{5}$$

where l is the length of the rigid bar and the inertial derivative of the vector $\boldsymbol{b}$ is calculated as:

$$\dot{\boldsymbol{b}} = \dot{\boldsymbol{\mathcal{B}}} b^{\mathcal{B}} + \boldsymbol{\mathcal{B}}\dot{b}^{\mathcal{B}} = \dot{\boldsymbol{\mathcal{B}}} b^{\mathcal{B}} = \boldsymbol{\mathcal{B}}\tilde{\omega}^{\mathcal{B}} b^{\mathcal{B}}. \tag{6}$$

Using the above two equations, the angular velocity of bar $\boldsymbol{\omega}_b$ can be written as (shown in [19]):

$$\boldsymbol{\omega}_b = \frac{\boldsymbol{b} \times \dot{\boldsymbol{b}}}{l^2}, \quad \boldsymbol{\omega}_b = \boldsymbol{\mathcal{B}} \begin{bmatrix}\omega_1^{\mathcal{B}} \\ \omega_2^{\mathcal{B}} \\ 0\end{bmatrix} = \boldsymbol{\mathcal{B}}\omega_b^{\mathcal{B}}. \tag{7}$$

and the angular momentum of bar $\boldsymbol{b}$ about its mass center can be written as:

$$\boldsymbol{h}_b = J_b \boldsymbol{\omega}_b, \quad J_b = \frac{m_b l^2}{12}, \tag{8}$$

$$\boldsymbol{h}_b = \frac{m_b}{12} \boldsymbol{b} \times \dot{\boldsymbol{b}}. \tag{9}$$

The angular momentum of the wheel of radius r_w, thickness l_w, the wheel spin speed $\omega_3^{\mathcal{B}}$, and the wheel angular velocity vector $\boldsymbol{\omega_w}$ are related by:

$$\boldsymbol{h}_w = \boldsymbol{\mathcal{B}} J_w^{\mathcal{B}} \omega^{\mathcal{B}}, \tag{10}$$

where

$$\boldsymbol{\omega}_w = \boldsymbol{\mathcal{B}} \begin{bmatrix} \omega_1^{\mathcal{B}} \\ \omega_2^{\mathcal{B}} \\ \omega_3^{\mathcal{B}} \end{bmatrix}, \quad J_w^{\mathcal{B}} = \begin{bmatrix} J_1 & 0 & 0 \\ 0 & J_1 & 0 \\ 0 & 0 & J_3 \end{bmatrix}, \tag{11}$$

$$J_1 = J_2 = \frac{m_w}{12}(3r_w^2 + l_w^2), \quad J_3 = \frac{1}{2} m_w r_w^2. \tag{12}$$

Using Eqs. (9) and (10), the total angular momentum vector of the joint member can be written in terms of $\boldsymbol{b}$ and $\dot{\boldsymbol{b}}$ as:

$$\boldsymbol{h} = \boldsymbol{h}_b + \boldsymbol{h}_w, \tag{13}$$

$$\boldsymbol{h} = \frac{m_b}{12} \boldsymbol{b} \times \dot{\boldsymbol{b}} + \boldsymbol{\mathcal{B}} J_w^{\mathcal{B}} \omega^{\mathcal{B}}, \tag{14}$$

$$\boldsymbol{h} = \left(\frac{m_b l^2}{12} + J_1 \right) \frac{\boldsymbol{b} \times \dot{\boldsymbol{b}}}{l^2} + \omega_3^{\mathcal{B}} J_3 \frac{\boldsymbol{b}}{l}, \tag{15}$$

$$\boldsymbol{h} = J_t \boldsymbol{b} \times \dot{\boldsymbol{b}} + J_a l \omega_3^{\mathcal{B}} \boldsymbol{b}, \tag{16}$$

where $J_t = \frac{m_b}{12} + \frac{J_1}{l^2}$, $J_a = \frac{J_3}{l^2}$.

Now, the inertial derivative of the angular momentum vector $\boldsymbol{h}$ is equal to the total torque about the mass center of the body. The resulting torque can be written as the sum of pure torques $\boldsymbol{\tau}$ and the torque due to the forces acting on the two ends of the bar:

$$\dot{\boldsymbol{h}} = \boldsymbol{\tau} + \frac{1}{2} \boldsymbol{b} \times (\boldsymbol{f}_2 - \boldsymbol{f}_1), \tag{17}$$

$$J_t \boldsymbol{b} \times \ddot{\boldsymbol{b}} + J_a l \dot{\omega}_3^{\mathcal{B}} \boldsymbol{b} + J_a l \omega_3^{\mathcal{B}} \dot{\boldsymbol{b}} = \boldsymbol{\tau} + \frac{1}{2} \boldsymbol{b} \times (\boldsymbol{f}_2 - \boldsymbol{f}_1). \tag{18}$$

Now, we write the above equation in inertial coordinates with $b = b^{\mathcal{E}}$ and $\omega_w = \omega_3^{\mathcal{B}}$ as:

$$J_t \tilde{b} \ddot{b} + J_a l \dot{\omega}_w b + J_a l \omega_w \dot{b} = \tau + \frac{1}{2} \tilde{b} (f_2 - f_1). \tag{19}$$

Similar to [19], a rigid bar length constraint of the following form is added:

$$b^{\mathsf{T}} b = l^2, \quad b^{\mathsf{T}} \dot{b} = 0, \quad b^{\mathsf{T}} \ddot{b} = -\dot{b}^{\mathsf{T}} \dot{b}. \tag{20}$$

The length constraint (Eq. (20)) appended with rotational dynamics (Eq. (19)) can be expressed in matrix form as:

$$\begin{bmatrix} \tilde{b} \\ b^{\mathsf{T}} \end{bmatrix} \ddot{b} = \begin{bmatrix} \frac{1}{J_t} \left(\tau + \frac{1}{2} \tilde{b} (f_2 - f_1) - J_a l \dot{\omega}_w b - J_a l \omega_w \dot{b} \right) \\ -\dot{b}^{\mathsf{T}} \dot{b} \end{bmatrix}. \tag{21}$$

The above linear algebra problem (Eq. (21)) has solution for $\ddot{b}$ if and only if the vector on the right hand side lies in the range space of the coefficient matrix:

$$\left(I - \frac{1}{l^2} \begin{bmatrix} \tilde{b} \\ b^{\mathsf{T}} \end{bmatrix} \begin{bmatrix} -\tilde{b} & b^{\mathsf{T}} \end{bmatrix} \right) \times \begin{bmatrix} \frac{1}{J_t} (\tau + \frac{1}{2} \tilde{b} (f_2 - f_1) - J_a l \dot{\omega}_w b - J_a l \omega_w \dot{b}) \\ -\dot{b}^{\mathsf{T}} \dot{b} \end{bmatrix} = 0, \tag{22}$$

where I is the identity matrix of the appropriate dimension. The above equation after further simplification reduces to:

$$\frac{b b^{\mathsf{T}} \tau}{l^2} - J_a l \dot{\omega}_w b - \frac{J_a l \omega_w b b^{\mathsf{T}} \dot{b}}{l^2} = 0, \tag{23}$$

which after using bar length constraint ($b^{\mathsf{T}} \dot{b} = 0$) becomes:

$$b^{\mathsf{T}} \tau = J_a l^3 \dot{\omega}_w. \tag{24}$$

Writing $\tau = \tau_{\parallel} + \tau_{\perp}$, where $\tau_{\parallel}$ is the component along the bar and $\tau_{\perp}$ is perpendicular to the bar, we get:

$$b^{\mathsf{T}} \tau_{\parallel} = J_a l^3 \dot{\omega}_w. \tag{25}$$

Also, since the coefficient matrix of $\ddot{b}$ in Eq. (21) has full column rank, there is a unique solution for $\ddot{b}$, which is given as:

$$J_t \ddot{b} = \frac{(l^2 I - b b^{\mathsf{T}})}{2 l^2} (f_2 - f_1) - \frac{\tilde{b} \tau}{l^2} + \frac{J_a \omega_w \tilde{b} \dot{b}}{l} - \frac{J_t b \dot{b}^{\mathsf{T}} \dot{b}}{l^2}. \tag{26}$$

Again using $\tau = \tau_{\parallel} + \tau_{\perp}$, we get the two final equations for rotational dynamics as:

$$J_t \ddot{b} = \frac{(l^2 I - b b^{\mathsf{T}})}{2 l^2} (f_2 - f_1) - \frac{\tilde{b} \tau_{\perp}}{l^2} + \frac{J_a \omega_w \tilde{b} \dot{b}}{l} - \frac{J_t b \dot{b}^{\mathsf{T}} \dot{b}}{l^2}, \tag{27}$$

$$b^{\mathsf{T}} \tau_{\parallel} = J_a l^3 \dot{\omega}_w. \tag{28}$$

The above equations represent the bar-wheel system rotational dynamics along with the bar length constraint.

Finally, the translational dynamics of the bar-wheel system can be written in inertial coordinates from Fig. 1 as:

$$(m_b + m_w) \ddot{r} = f_1 + f_2, \tag{29}$$

where m_b and m_w are the mass of the bar and mass of the wheel, respectively. The translational dynamics (Eq. (29)) together with rotational dynamics (Eqs. (27-28)), fully describes the motion of the bar-gyro member.

The mass in the strings can be modelled by dividing the mass of the string into several point masses. This is achieved by adding string-to-string nodes that have the associated mass of the string. String-to-string nodes only have string-end connections and thus no bar-end is present at string-to-string node, e.g.: node n_7 in Fig. 2. The dynamics for such nodes can be written as:

$$m_s \ddot{r}_s = f_s, \tag{30}$$

where m_s is the mass of the point node and r_s is the position vector of the node.

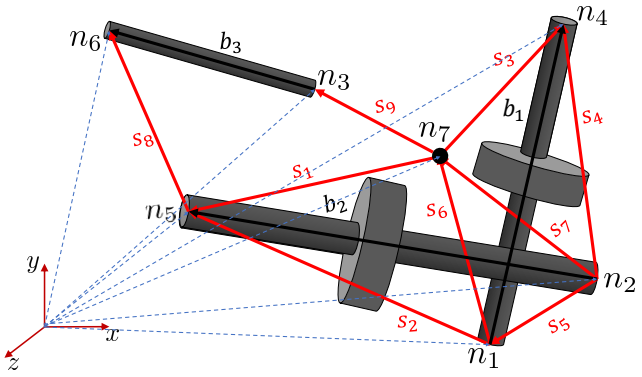

Fig. 2. General tensegrity system representation with nodal matrices $N_1 = [n_1\ n_2\ n_3]$, $N_2 = [n_4\ n_5\ n_6]$, and $N_s = [n_7]$. Bar matrix $B = [b_1\ b_2\ b_3]$ and string matrix $S = [s_1\ s_2\ \cdots\ s_9]$ are also shown.

IV. Matrix Form of the System Dynamics

The aim of this section is to write the system dynamics in a compact matrix form for assumed β number of bar-wheel member. Let us denote the node position vector: $n_i = [n_{ix}\ n_{iy}\ n_{iz}]^\mathsf{T} \in \mathbb{R}^{3\times 1}$ and the matrix containing the position of the nodes at the base of a bar vector as $N_1 = \begin{bmatrix} n_1 & n_2 & \cdots & n_\beta \end{bmatrix} \in \mathbb{R}^{3\times\beta}$, the position of the nodes at the terminal ends of the bar vectors as $N_2 = \begin{bmatrix} n_{1+\beta} & n_{2+\beta} & \cdots & n_{2\beta} \end{bmatrix} \in \mathbb{R}^{3\times\beta}$, and the string-to-string nodes to be stacked similarly in $N_s \in \mathbb{R}^{3\times\sigma}$, as shown in Fig. 2. So the full node matrix can consequently be split as $N = \begin{bmatrix} N_1 & N_2 & N_s \end{bmatrix} \in \mathbb{R}^{3\times(2\beta+\sigma)}$ where σ is the number of string-to-string nodes. Let us also define matrix $B = \begin{bmatrix} b_1 & b_2 & \cdots & b_\beta \end{bmatrix} \in \mathbb{R}^{3\times\beta}$, where each column represents the bar vector b_i. This convention yields $B = NC_b^\mathsf{T}$ with $C_b = \begin{bmatrix} -I_\beta & I_\beta & 0 \end{bmatrix} \in \mathbb{R}^{\beta\times(2\beta+\sigma)}$ as a bar connectivity matrix describing which two nodes form a particular bar and $I_\beta \in \mathbb{R}^{\beta\times\beta}$ is the identity matrix. Similarly, we define $R = NC_r^\mathsf{T} \in \mathbb{R}^{3\times\beta}$ with $C_r = 1/2\begin{bmatrix} I_\beta & I_\beta & 0 \end{bmatrix} \in \mathbb{R}^{\beta\times(2\beta+\sigma)}$ and each vector in R represents the center position vector r_i.

To write the dynamics in a compact matrix form, we take each term in Eq. (27) and arrange them as a vector in a matrix, e.g. $J_t = \begin{bmatrix} J_{t,1} & J_{t,2} & \cdots & J_{t,\beta} \end{bmatrix}^\mathsf{T} \in \mathbb{R}^{\beta\times 1}$. Then, the left side of Eq. (27) is the i^{th} column of the matrix $\ddot{B}\hat{J}_t$:

$$\ddot{B}\hat{J}_t = \begin{bmatrix} J_{t,1}\ddot{b}_1 & J_{t,2}\ddot{b}_2 & \cdots & J_{t,\beta}\ddot{b}_\beta \end{bmatrix}, \tag{31}$$

where the "hat" operator over a vector forms a diagonal matrix from the elements of the vector.

This process can similarly be performed for the remaining terms in Eq. (27), as summarized below. Similar to N, we can define $F \in \mathbb{R}^{3\times(2\beta+\sigma)}$ containing its columns as the total force vector acting on the i^{th} node n_i. Converting the $\frac{1}{2}(f_2 - f_1)$ term into a matrix form, we get:

$$\frac{1}{2}(f_2 - f_1) \longrightarrow \frac{1}{2}FC_b^\mathsf{T}, \tag{32}$$

$$-\frac{1}{2l^2}bb^\mathsf{T}(f_2 - f_1) \longrightarrow -B\frac{1}{2}\hat{l}^{-2}\lfloor B^\mathsf{T}FC_b^\mathsf{T}\rfloor, \tag{33}$$

where we introduce the $\lfloor\circ\rfloor$ operator, which sets every off-diagonal element of the square matrix operand to zero. Similarly, the other terms can be written as:

$$\frac{J_a}{l}\omega_w\tilde{b}\dot{b} \longrightarrow \tilde{B}\hat{\dot{B}}\hat{J}_a\hat{\omega}_w\hat{l}^{-1}, \tag{34}$$

with $\tilde{B} \triangleq \begin{bmatrix} \tilde{b}_1 & \tilde{b}_2 & \cdots & \tilde{b}_\beta \end{bmatrix} \in \mathbb{R}^{3\times 3\beta}$, where $\tilde{b}_i$ is a skew-symmetric matrix formed using the elements of the vector b_i, and

$$-\frac{\tilde{b}\tau_\perp}{l^2} \longrightarrow -\tilde{B}\hat{\mathcal{T}}\hat{l}^{-2}, \tag{35}$$

$$-\frac{J_t}{l^2}b\dot{b}^\mathsf{T}\dot{b} \longrightarrow -B\hat{J}_t\hat{l}^{-2}\lfloor\dot{B}^\mathsf{T}\dot{B}\rfloor. \tag{36}$$

Substituting for matrix expressions from Eqs. (31-36) in Eq. (27), the following full matrix expression for $\ddot{B}$ is obtained as:

$$\ddot{B}\hat{J}_t = \frac{1}{2}FC_b^\mathsf{T} - \frac{1}{2}B\hat{l}^{-2}\lfloor B^\mathsf{T}FC_b^\mathsf{T}\rfloor - \tilde{B}\hat{\mathcal{T}}\hat{l}^{-2} + \tilde{B}\hat{\dot{B}}\hat{J}_a\hat{\omega}_w\hat{l}^{-1} - B\hat{J}_t\hat{l}^{-2}\lfloor\dot{B}^\mathsf{T}\dot{B}\rfloor, \tag{37}$$

which can be further simplified with the following definition of $\hat{\lambda} \in \mathbb{R}^{\beta\times\beta}$ as:

$$\hat{\lambda} = -\hat{J}_t\hat{l}^{-2}\lfloor\dot{B}^\mathsf{T}\dot{B}\rfloor - \frac{1}{2}\hat{l}^{-2}\lfloor B^\mathsf{T}FC_b^\mathsf{T}\rfloor, \tag{38}$$

$$\ddot{B}\hat{J}_t = \frac{1}{2}FC_b^\mathsf{T} + B\hat{\lambda} - \tilde{B}\hat{\mathcal{T}}\hat{l}^{-2} + \tilde{B}\hat{\dot{B}}\hat{J}_a\hat{\omega}_w\hat{l}^{-1}. \tag{39}$$

Finally, writing Eq. (28) into a matrix form, with $\tau_\parallel = \frac{b}{l}\tau_b$, where τ_b is scalar representing the torque along the bar, we get:

$$\tau_b = J_a l^2\dot{\omega}_w \longrightarrow \tau_B = \hat{J}_a\hat{l}^2\dot{\omega}_W, \tag{40}$$

where $\tau_B = [\tau_{b1}\ \tau_{b2}\cdots\tau_{b\beta}]^\mathsf{T} \in \mathbb{R}^{\beta\times 1}$ and $\dot{\omega}_W = [\dot{\omega}_{w1}\ \dot{\omega}_{w2}\cdots\dot{\omega}_{w\beta}]^\mathsf{T} \in \mathbb{R}^{\beta\times 1}$.

The translational dynamics must similarly be converted into a matrix expression as:

$$(m_b + m_w)\ddot{r} = f_1 + f_2 \longrightarrow \ddot{R}\hat{m}_t = 2FC_r^\mathsf{T}. \tag{41}$$

Similarly, the dynamics of the string-to-string node can be put into a matrix form as:

$$m_s\ddot{r}_s = f_s \longrightarrow \ddot{R}_s\hat{m}_s = F_s. \tag{42}$$

Note that the bar and string nodes can be extracted from the node matrix N with two new definitions of matrix $N_b \in \mathbb{R}^{3\times 2\beta}$ and matrix $N_s \in \mathbb{R}^{3\times\sigma}$ as:

$$N_b = \begin{bmatrix} N_1 & N_2 \end{bmatrix} = N\begin{bmatrix} I_{2\beta} \\ 0 \end{bmatrix} = NC_{nb}^\mathsf{T}, \tag{43}$$

$$N_s = N\begin{bmatrix} 0 \\ I_\sigma \end{bmatrix} = NC_{ns}^\mathsf{T}. \tag{44}$$

Similar to bar connectivity matrix, we now define string connectivity matrix $C_s \in \mathbb{R}^{\alpha\times(2\beta+\sigma)}$, where α is the number of strings. The matrix C_s can be separated

into two parts: $C_{sb} \in \mathbb{R}^{\alpha\times 2\beta}$, for bar-to-string joints, and $C_{ss} \in \mathbb{R}^{\alpha\times\sigma}$, for string-to-string joints:

$$S = NC_s^{\mathsf{T}} = \begin{bmatrix} N_b & N_s \end{bmatrix} \begin{bmatrix} C_{sb}^{\mathsf{T}} \\ C_{ss}^{\mathsf{T}} \end{bmatrix} \in \mathbb{R}^{3\times\alpha}. \tag{45}$$

After formulating matrix forms in Eqs. (39-42), we combine them together as:

$$\begin{aligned} &\begin{bmatrix} \ddot{B} & \ddot{R}_b & \ddot{R}_s \end{bmatrix} \begin{bmatrix} \hat{J}_t & 0 & 0 \\ 0 & \hat{m}_t & 0 \\ 0 & 0 & \hat{m}_s \end{bmatrix} \\ &\qquad + \begin{bmatrix} B & R_b & R_s \end{bmatrix} \begin{bmatrix} -\hat{\lambda} & 0 & 0 \\ 0 & 0 & 0 \\ 0 & 0 & 0 \end{bmatrix} \\ &= F \begin{bmatrix} \frac{1}{2}C_b^{\mathsf{T}} & 2C_r^{\mathsf{T}} & 0 \\ 0 & 0 & I \end{bmatrix} + \begin{bmatrix} \tilde{B}\hat{\dot{B}}\hat{J}_a\hat{\omega}_w\hat{l}^{-1} - \tilde{B}\hat{\mathcal{T}}\hat{l}^{-2} & 0 & 0 \end{bmatrix}. \end{aligned} \tag{46}$$

The following identity:

$$\begin{bmatrix} \frac{1}{2}C_b^{\mathsf{T}} & 2C_r^{\mathsf{T}} & 0 \\ 0 & 0 & I \end{bmatrix}^{-1} = \begin{bmatrix} C_b & 0 \\ C_r & 0 \\ 0 & I \end{bmatrix}, \tag{47}$$

can be used in Eq. (46) to get:

$$\begin{aligned} &\begin{bmatrix} \ddot{B} & \ddot{R}_b & \ddot{R}_s \end{bmatrix} \begin{bmatrix} \hat{J}_t & 0 & 0 \\ 0 & \hat{m}_t & 0 \\ 0 & 0 & \hat{m}_s \end{bmatrix} \begin{bmatrix} C_b & 0 \\ C_r & 0 \\ 0 & I \end{bmatrix} + \\ &\qquad \begin{bmatrix} B & R_b & R_s \end{bmatrix} \begin{bmatrix} -\hat{\lambda} & 0 & 0 \\ 0 & 0 & 0 \\ 0 & 0 & 0 \end{bmatrix} \begin{bmatrix} C_b & 0 \\ C_r & 0 \\ 0 & I \end{bmatrix} \\ &= F + \begin{bmatrix} \tilde{B}\hat{\dot{B}}\hat{J}_a\hat{\omega}_w\hat{l}^{-1} - \tilde{B}\hat{\mathcal{T}}\hat{l}^{-2} & 0 & 0 \end{bmatrix} \begin{bmatrix} C_b & 0 \\ C_r & 0 \\ 0 & I \end{bmatrix}, \end{aligned} \tag{48}$$

and after using the previously defined expressions:

$$\begin{bmatrix} B & R_b & R_s \end{bmatrix} = N \begin{bmatrix} C_{nb}^{\mathsf{T}}C_b^{\mathsf{T}} & C_{nb}^{\mathsf{T}}C_r^{\mathsf{T}} & C_{ns}^{\mathsf{T}} \end{bmatrix}, \tag{49}$$

we get:

$$\begin{aligned} &\ddot{N} \begin{bmatrix} C_{nb}^{\mathsf{T}}C_b^{\mathsf{T}} & C_{nb}^{\mathsf{T}}C_r^{\mathsf{T}} & C_{ns}^{\mathsf{T}} \end{bmatrix} \begin{bmatrix} \hat{J}_t & 0 & 0 \\ 0 & \hat{m}_t & 0 \\ 0 & 0 & \hat{m}_s \end{bmatrix} \begin{bmatrix} C_b & 0 \\ C_r & 0 \\ 0 & I \end{bmatrix} \\ &+ N \begin{bmatrix} C_{nb}^{\mathsf{T}}C_b^{\mathsf{T}} & C_{nb}^{\mathsf{T}}C_r^{\mathsf{T}} & C_{ns}^{\mathsf{T}} \end{bmatrix} \begin{bmatrix} -\hat{\lambda} & 0 & 0 \\ 0 & 0 & 0 \\ 0 & 0 & 0 \end{bmatrix} \begin{bmatrix} C_b & 0 \\ C_r & 0 \\ 0 & I \end{bmatrix} \\ &= F + \begin{bmatrix} \tilde{B}\hat{\dot{B}}\hat{J}_a\hat{\omega}_w\hat{l}^{-1} - \tilde{B}\hat{\mathcal{T}}\hat{l}^{-2} & 0 & 0 \end{bmatrix} \begin{bmatrix} C_b & 0 \\ C_r & 0 \\ 0 & I \end{bmatrix}. \end{aligned} \tag{50}$$

Now, let us define "force density" γ_i as the tension per unit length in the i^{th} string s_i. The tension vector in the string can be now be written as $\mathrm{t}_i = \mathrm{s}_i\gamma_i$. Combining the tension vectors, the matrix of string tensions $T \in \mathbb{R}^{3\times\alpha}$ is written as:

$$T = [t_1\ t_2\ \cdots\ t_\alpha] = S\hat{\gamma} = NC_s^{\mathsf{T}}\hat{\gamma}, \tag{51}$$

and the internal forces acting on nodes caused by string tensions are calculated as $NC_s^{\mathsf{T}}\hat{\gamma}C_s$. Let us also define w_i as the i^{th} column of the matrix $W \in \mathbb{R}^{3\times(2\beta+\sigma)}$, where w_i is the external force acting on the node n_i.The full force matrix expression can then be written as:

$$F = \begin{bmatrix} F_b & F_s \end{bmatrix} = W - NC_s^{\mathsf{T}}\hat{\gamma}C_s. \tag{52}$$

Substituting Eq. (52) for F, and rearranging yields the following expression for the full system dynamics:

$$\begin{aligned} &\ddot{N} \begin{bmatrix} C_{nb}^{\mathsf{T}}C_b^{\mathsf{T}}\hat{J}_tC_b + C_{nb}^{\mathsf{T}}C_r^{\mathsf{T}}\hat{m}_tC_r & C_{ns}^{\mathsf{T}}\hat{m}_s \end{bmatrix} \\ &\qquad + N \begin{bmatrix} C_s^{\mathsf{T}}\hat{\gamma}C_{sb} - C_{nb}^{\mathsf{T}}C_b^{\mathsf{T}}\hat{\lambda}C_b & C_s^{\mathsf{T}}\hat{\gamma}C_{ss} \end{bmatrix} \\ &\qquad = W + \begin{bmatrix} (\tilde{B}\hat{\dot{B}}\hat{J}_a\hat{\omega}_w\hat{l}^{-1} - \tilde{B}\hat{\mathcal{T}}\hat{l}^{-2})C_b & 0 \end{bmatrix}, \end{aligned} \tag{53}$$

which can be written in compact matrix form with the following definitions of M_s, K_s, and W_T as:

$$\ddot{N}M_s + NK_s = W_T, \tag{54}$$

$$\tau_B = \hat{J}_a\hat{l}^2\dot{\omega}_W, \tag{55}$$

where

$$M_s = \begin{bmatrix} C_{nb}^{\mathsf{T}}(C_b^{\mathsf{T}}\hat{J}_tC_b + C_r^{\mathsf{T}}\hat{m}_tC_r) & C_{ns}^{\mathsf{T}}\hat{m}_s \end{bmatrix}, \tag{56}$$

$$K_s = \begin{bmatrix} C_s^{\mathsf{T}}\hat{\gamma}C_{sb} - C_{nb}^{\mathsf{T}}C_b^{\mathsf{T}}\hat{\lambda}C_b & C_s^{\mathsf{T}}\hat{\gamma}C_{ss} \end{bmatrix}, \tag{57}$$

$$\hat{\lambda} = -\hat{J}_t\hat{l}^{-2}\lfloor\dot{B}^{\mathsf{T}}\dot{B}\rfloor - \frac{1}{2}\hat{l}^{-2}\lfloor B^{\mathsf{T}}(W - NC_s^{\mathsf{T}}\hat{\gamma}C_s)C_b^{\mathsf{T}}\rfloor, \tag{58}$$

$$W_T = W + \begin{bmatrix} (\tilde{B}\hat{\dot{B}}\hat{J}_a\hat{\omega}_w\hat{l}^{-1} - \tilde{B}\hat{\mathcal{T}}\hat{l}^{-2})C_b & 0 \end{bmatrix}, \tag{59}$$

$\tau_B = [\tau_{b1}\ \tau_{b2}\cdots\tau_{b\beta}]^{\mathsf{T}}$ and $\dot{\omega}_W = [\dot{\omega}_{w1}\ \dot{\omega}_{w2}\cdots\dot{\omega}_{w\beta}]^{\mathsf{T}}$.

V. Class-K Tensegrity Systems

In class-k tensegrity systems, multiple bars are connected (ball joint) at a node such that there is no torque/moment transfer from one bar member to any other bar member. The structure is said to be of class-1 if the maximum number of bars present at any nodes is one and class-k if the maximum number of bars present at any node is k [2]. The dynamics of class-k tensegrity structures (for $k > 1$) can be easily extended from the formulation developed in the previous section. Each class-k joint can be handled by creating $k-1$ virtual nodes which are constrained to coincide at all times with the use of Lagrange constraint forces. These constraints are written as:

$$NP = D, \tag{60}$$

where $P \in \mathbb{R}^{(2\beta+\sigma)\times c}$ and $D \in \mathbb{R}^{3\times c}$ are specified such that constrained nodes coincide at all times and the number of added constraints is denoted as c. Adding the linear constraints introduce Lagrange constraint forces (ΩP^{T}) resulting in the new dynamics:

$$\ddot{N}M_s + NK_s = W_T + \Omega P^{\mathsf{T}}, \tag{61}$$

where $\Omega \in \mathbb{R}^{3\times c}$ is a matrix of Lagrange multipliers satisfying the dynamics constraints at all time-steps and

the force density in the bars changes according to the following equation:

$$\hat{\lambda} = -\hat{J}\hat{l}^{-2}\lfloor \dot{B}^{\mathsf{T}}\dot{B}\rfloor - \frac{1}{2}\hat{l}^{-2}\lfloor B^{\mathsf{T}}(W + \Omega P^{\mathsf{T}} - S\hat{\gamma}C_s)C_{nb}^{\mathsf{T}}C_b^{\mathsf{T}}\rfloor. \quad (62)$$

A. Reduced-order dynamics

The added constraints reduced the order of the system dynamics to a smaller dimension manifold. Here, we use the same procedure developed in [19] by starting with the constraint equation (Eq. (60)):

$$NP = NU\Sigma V^{\mathsf{T}} = [\eta_1 \;\; \eta_2]\begin{bmatrix}\Sigma_1\\ 0\end{bmatrix}[V^{\mathsf{T}}] = D, \quad (63)$$

where the matrices U, Σ, and V are numerically generated by performing the Singular Value Decomposition (SVD) of the full column rank matrix P as $P = U\Sigma V^{\mathsf{T}} = [U_1 \;\; U_2]\begin{bmatrix}\Sigma_1\\ 0\end{bmatrix}[V^{\mathsf{T}}]$, and $[\eta_1 \;\; \eta_2] \triangleq NU$, to get:

$$\eta_1 = DV\Sigma_1^{-1}, \;\; \dot{\eta}_1 = 0, \;\; \ddot{\eta}_1 = 0. \quad (64)$$

The constant value of variable η_1 represents the constraint space (no-motion space) and η_2 represents the reduced space in the new coordinate system. The dynamics equation (Eq. (61)) can now be rewritten as:

$$\ddot{N}UU^{\mathsf{T}}M_s + NUU^{\mathsf{T}}K_s = W_T + \Omega V\Sigma^{\mathsf{T}}U^{\mathsf{T}}, \quad (65)$$

$$\ddot{\eta}_2U_2^{\mathsf{T}}M_s + \eta_1U_1^{\mathsf{T}}K_s + \eta_2U_2^{\mathsf{T}}K_s = W_T + \Omega V\Sigma_1^{\mathsf{T}}U_1^{\mathsf{T}}. \quad (66)$$

Post-multiplying the above equation by a non-singular matrix $[M_s^{-1}U_1 \;\; U_2]$ will result in two parts, where the first part gives an algebraic equation that is used to solve for the Lagrange multiplier:

$$NK_sM_s^{-1}U_1 - \Omega P^{\mathsf{T}}M_s^{-1}U_1 = W_TM_s^{-1}U_1, \quad (67)$$

and the second part gives a second-order matrix differential equation for the reduced order dynamics:

$$\ddot{\eta}_2U_2^{\mathsf{T}}M_sU_2 + \eta_2U_2^{\mathsf{T}}K_sU_2 = W_TU_2 - \eta_1U_1^{\mathsf{T}}K_sU_2. \quad (68)$$

VI. Simulation and Experimental Setup

The experimental setup shown in Fig. 3 is a planar D-bar tensegrity structure [2] with gimbal motors (T-MOTOR GB54-1) attached to each of the four 12 inch wooden bars (shown in black). Each bar in the system is connected to two other bars through a hinge joint which is allowed to slide along the vertical and horizontal straight lines. The shape (D-bar angle) and orientation of the D-bar structure is controlled by the strings, as shown in Fig. 3. The IMU sensor (BWT61CL Bluetooth MPU6050) is used to measure the angular rotation of the structure. The material used for the strings is spectra (UHMWPE). The strings are passed through 3D printed pulleys (green) to reduce the amount of friction. Both the horizontal strings are independently controlled by two MX-12W DYNAMIXEL servo motors attached to the pulleys. ARDUINO MEGA2560 was used to communicate and control the gyro motors by a C++ script, and dynamixel servos were controlled by its embedded driver through a python script.

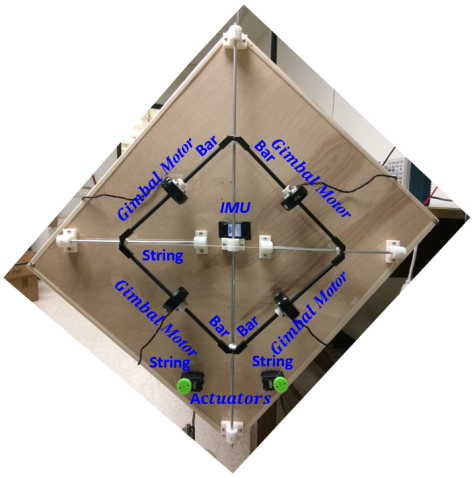

Fig. 3. Experimental setup for gyroscopic tensegrity D-bar structure.

Figure 4 shows the same setup to perform a dynamic simulation with the initial configuration in XY-plane. The initial configuration is an equilibrium configuration with no prestress in the horizontal strings and gyro wheels rotating at a constant speed of 715 rpm. The angular momentum vector for each bar-wheel system is also shown in Fig. 4 to give the sense of direction of wheel rotation.

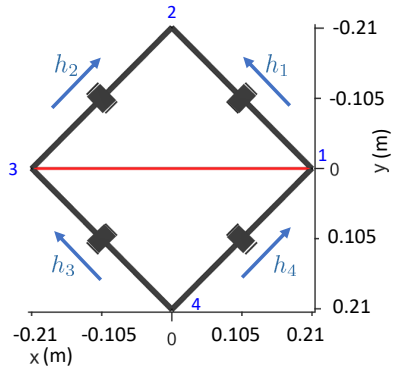

Fig. 4. Simulation setup for gyroscopic tensegrity D-bar structure.

The dynamic simulation on gyroscopic D-bar tensegrity structure was performed by reducing the distance between node-1 and node-3 to 1/3 of the initial distance. The three time-lapse images of the dynamic simulation for time $t = 0$ sec, $t = 1.5$ sec, and $t = 3$ sec are shown in Fig. 5. These configurations are shown by looking at YZ-plane to distinctly show the change in orientation of the plane containing the D-bar structure. The rotation of the plane by changing the length of the strings (hence, the direction of the angular momentum vector) can also be understood by the conservation

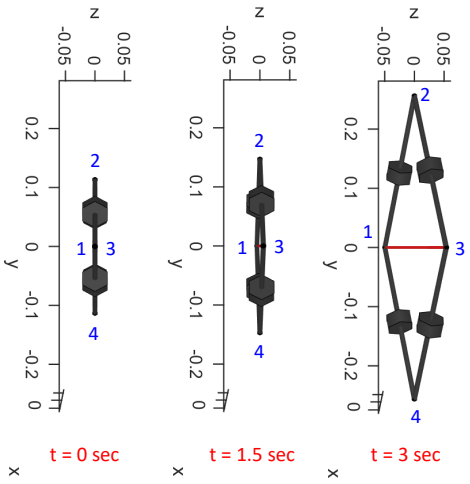

Fig. 5. Dynamic simulation time-lapse of gyroscopic tensegrity D-bar structure with rotating wheel.

of the angular momentum of the system. A similar change in the orientation of the plane was observed in the experiment performed by reducing the length of the horizontal strings. Three time-lapse images of the experiment are shown in Fig. 6, which agrees with the proposed approach to control the attitude and derived dynamics of the gyroscopic tensegrity structures.

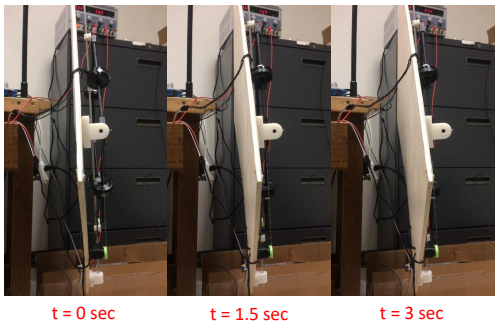

Fig. 6. Experimental setup time-lapse of gyroscopic tensegrity D-bar structure with rotating wheel.

Figure 7 shows the time history of variation in x,y, and z coordinates of all the four nodes performed using dynamic simulation. As the length of the horizontal string is reduced, x-coordinate of nodes n_1 and n_3 varies (closer) while nodes n_2 and n_4 moves (away) in y-direction. Due to the presence of gyroscopic forces in Fig. 7(a), a significant motion was observed in the z-direction. Nodes n_1 and n_3 were observed to have a displacement of ≈2cm in z-direction, which qualitatively matches the experimental results from Fig. 6. No motion was observed in z-direction for the case of zero gyroscopic wheels spin speed as shown in Fig. 7(b).

Figure 8(a) plots the variation in z-coordinate of all the four nodes obtained from the experimental results with the specified wheel spin speed. Figure 8(a) shows substantial motion in z-direction for nodes n_1 and n_3,

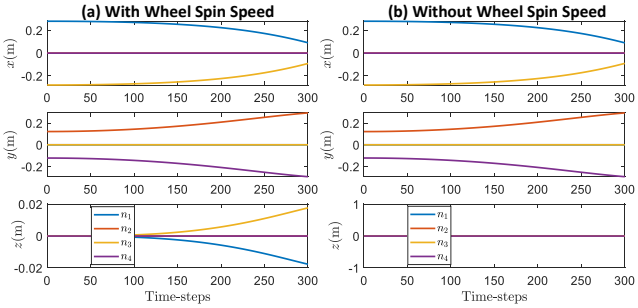

Fig. 7. Simulation result with variation in x,y, and z coordinates of all the four nodes with time.

which was calculated from the angular measurement data obtained from the onboard IMU. The motion of the nodes in the z-direction follows the same trend, but a smaller displacement is observed due to the added (unaccounted) inertia of the entire setup. Figure 8(b) plots the variation in z-coordinate with zero wheel spin speed. No significant motion (rotation) was observed in the absence of gyroscopic forces. This validates our approach to construct the experimental setup and shows a good match with the simulation and experimental results.

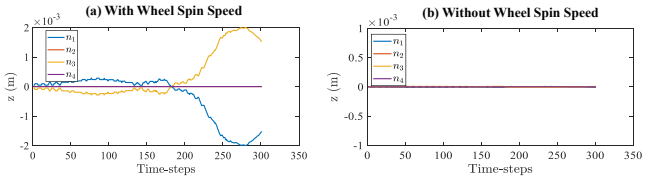

Fig. 8. Experimental result with variation in x,y, and z coordinates of all the four nodes with time.

Figure 9 provides the plot for error in satisfying bar length constraints with the time-steps of the simulation. The error in constraint violation is of the order 10^{-15} representing the accuracy of the formulated dynamics that avoids transcendental functions.

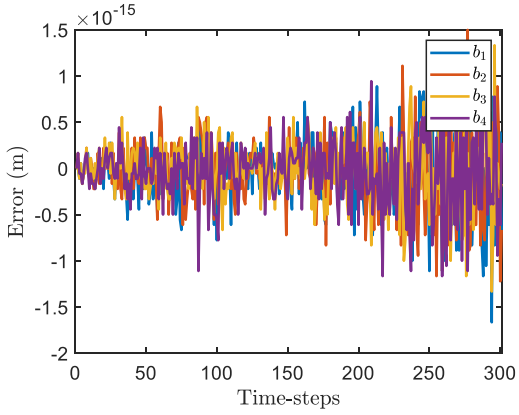

Fig. 9. Plot for error in bar length constraint for all time-steps.

VII. CONCLUSIONS

The paper provided a systematic approach to derive the dynamics of any tensegrity system with gyroscopic wheels attached to its bars. The second-order matrix differential equation along with a second-order vector differential equation describes the equations of motion in the presence of external forces and torques on the bars. The matrix differential equation provides the information on position and orientation of the bar, and the vector differential equation provides the information on the angular position of the wheels. A reduced-order model is also developed for the class-k tensegrity structures to increase the accuracy and computational efficiency of the formulation. Finally, it was shown that the orientation of the structure could be controlled by controlling the shape, i.e., by controlling the length of the stings. This paper formulates the mechanics of gyroscopic tensegrity systems and paves the path to form control principles associated with the design, development, and control of such structures.

ACKNOWLEDGMENT

The authors would like to thank Mr. Ran Wang for his help in setting up the experiment.

References

[1] H. Lalvani, "Origins of tensegrity: Views of emmerich, fuller and snelson," International Journal of Space Structures, vol. 11, no. 1-2, p. 27, 1996. [Online]. Available: http://sps.sagepub.com/content/11/1-2/27.short

[2] R. Skelton and M. de Oliveira, Tensegrity Systems. Springer US, 2009.

[3] R. Goyal, E. A. P. Hernandez, and R. E. Skelton, "Analytical study of tensegrity lattices for mass-efficient mechanical energy absorption," International Journal of Space Structures, pp. 1–19, 2019.

[4] V. SunSpiral, G. Gorospe, J. Bruce, A. Iscen, G. Korbel, S. Milam, A. Agogino, and D. Atkinson, "Tensegrity based probes for planetary exploration: Entry, descent and landing (edl) and surface mobility analysis," International Journal of Planetary Probes, vol. 7, 2013.

[5] A. Amendola, G. Carpentieri, M. de Oliveira, R. Skelton, and F. Fraternali, "Experimental investigation of the softening–stiffening response of tensegrity prisms under compressive loading," Composite Structures, vol. 117, pp. 234 – 243, 2014.

[6] K. Caluwaerts, J. Despraz, A. Işçen, A. P. Sabelhaus, J. Bruce, B. Schrauwen, and V. SunSpiral, "Design and control of compliant tensegrity robots through simulation and hardware validation," Journal of The Royal Society Interface, vol. 11, no. 98, 2014.

[7] C. Paul, F. J. Valero-Cuevas, and H. Lipson, "Design and control of tensegrity robots for locomotion," IEEE Transactions on Robotics, vol. 22, no. 5, pp. 944–957, 2006.

[8] H. Karnan, R. Goyal, M. Majji, R. E. Skelton, and P. Singla, "Visual feedback control of tensegrity robotic systems," 2017 IEEE/RSJ-IROS, pp. 2048–2053, Sept 2017.

[9] G. Carpentieri, R. E. Skelton, and F. Fraternali, "Minimum mass and optimal complexity of planar tensegrity bridges," International Journal of Space Structures, vol. 30, no. 3-4, pp. 221–243, 2015.

[10] K. Nagase and R. E. Skelton, "Minimal mass tensegrity structures," Journal of the International Association for Shell and Spatial Structures, vol. 55, no. 1, pp. 37–48, 2014.

[11] D. E. Ingber, "The architecture of life," Scientific America, vol. 278, no. 1, pp. 48–57, 1998.

[12] J. Despraz, "Super ball bot, structures for planetary landing and exploration," Master's thesis, NASA Ames Research Center, 2013.

[13] B. Wie, Space vehicle dynamics and control. American Institute of Aeronautics and Astronautics, 2008.

[14] P. C. Hughes, Spacecraft Attitude Dynamics. Wiley & Sons, New York, 1986.

[15] A. M. Giordano, C. Ott, and A. Albu-Schäffer, "Coordinated control of spacecraft's attitude and end-effector for space robots," IEEE Robotics and Automation Letters, vol. 4, no. 2, pp. 2108–2115, 2019.

[16] C. M. Roithmayer, "International space station attitude control and energy storage experiment: Effects of flywheel torque," NASA Technical Report, 1999.

[17] S. R. Vadali and H.-S. Oh, "Space station attitude control and momentum management: A nonlinear look," Journal of Guidance, Control and Dynamics, vol. 15, no. 3, 1992.

[18] R. Goyal, T. Bryant, M. Majji, R. E. Skelton, and A. Longman, "Design and control of growth adaptable artificial gravity space habitat," in AIAA SPACE and Astronautics Forum and Exposition, 2017, p. 5141.

[19] R. Goyal and R. E. Skelton, "Tensegrity system dynamics with rigid bars and massive strings," Multibody System Dynamics, vol. 46(3), pp. 203–228, 2019.